Available online at www.sciencedirect.com
SCIENCE DIRECT
Polymer 46 (2005) 6719–6725
polymer
www.elsevier.com/locate/polymer

Description and modeling of fiber orientation in injection molding of fiber reinforced thermoplastics

Michel Vincent[a,*], T. Giroud[a], A. Clarke[b], C. Eberhardt[b]

[a]Ecole des Mines de Paris, CEMEF, UMR CNRS 7635, BP 207, 06904 Sophia Antipolis Cedex, France
[b]Department of Physics and Astronomy, Molecular Physics and Instrumentation Group, University of Leeds, Leeds LS2 9JT, UK

Available online 24 May 2005

Abstract

As mechanical properties of short fiber reinforced thermoplastic injected components depend on flow induced fiber orientation, there is considerable interest in validating and improving models which link the flow field and fiber orientations to mechanical properties. The present paper concerns firstly the observation and quantification of fiber orientation in a rectangular plaque with adjustable thickness and molded with 30 and 50 wt% short fiber reinforced polyarylamide. An automated 2D optical technique has been used to determine fiber orientations. A classical skin (with orientation parallel to the flow)–core (with orientation perpendicular) structure is observed for thick plaques (thickness greater than 3 mm) but the core region is fragmentary for thickness less than 1.7 mm. It is shown that the gate design and different levels of fiber interactions, due to different fiber concentrations, are responsible for these observations. Secondly, computer simulations of flow and fiber orientation are shown. The agreement with the actual data is good, except in the case of the core for thin plaques. The limitations that have to be resolved come not only from the standard fiber orientation equations, but also from the flow kinematics computation.

Keywords: Fiber reinforced thermoplastics; Injection molding; Fiber orientation quantification

1. Introduction

Fiber reinforced thermoplastics are semi-products obtained by mixing polymer and fibers in an extruder, and pelletizing. The fiber content is generally between 20 and 50 wt%, the fiber length is around 500 μm, and the diameter around 15 μm. They can be processed like any other thermoplastic, by injection molding for instance. As mechanical properties depend on flow induced fiber orientation, there is considerable interest in establishing relationships between flow and orientation, and numerically predicted fiber orientation to mechanical properties. The present paper concerns the observation and computation of fiber orientation.

Most observations in injected parts show two skin layers with preferential orientation parallel to the flow direction, and a core region with orientation perpendicular to the flow and in the plane of the part (see a review in Ref. [1]). It is known that in a pure shear flow, fibers orient mainly in the flow direction, whereas in extensional flows, they orient in the direction of extension. Most injected parts have a nearly constant thickness, which is much lower that the other dimensions. Therefore, shear deformations are dominant, and this explains the skin layers. A divergent flow is responsible for the core layer. This happens at the gate that is at the junction between the feeding channel and the cavity itself, whose cross-section is larger than that of the channel. Section 2 will present measurement and quantification of fiber orientation.

Prediction of fiber orientation during injection molding is an important challenge. Local anisotropic mechanical properties can be deduced, improving structural computation precision for part design. The motions of individual fibers, or of a lot of fibers interacting with each other, have been studied both experimentally and theoretically. Section 3 will present fiber orientation computations used in injection molding.

* Corresponding author. Tel.: +33 4 93 95 74 12; fax: +33 4 92 38 97 52.
E-mail address: michel.vincent@ensmp.fr (M. Vincent).

0032-3861/$ - see front matter © 2005 Elsevier Ltd. All rights reserved.
doi:10.1016/j.polymer.2005.05.026

2. Observation and quantification of fiber orientation

2.1. Material and molding conditions

Two commercial polyarylamide samples provided by Solvay with short glass fiber weight fractions of 30% (Ixef 1002) and 50% (Ixef 1022) were investigated. They will be called PAA30 and PAA50. The fiber diameter is 10 μm, and the average length is 200 μm. Moldings were performed in a fan-gated rectangular mold 200 mm long and 40 mm wide, as shown in Fig. 1. Its thickness can be varied: 1.1, 1.7, 3, 5 mm. The gate region geometry is indicated on Fig. 1(b) and (c).

The standard molding conditions are: flow rate: 15 cm^3/s; mold temperature 130 °C; melt temperature 40 °C; packing pressure: 40 MPa; packing time: 15 s. Other molding conditions have been tested by changing one parameter, the other ones remaining at the so call standard value. The flow rate was set to 6 and 24 cm^3/s, packing pressure to 10 and 85 MPa, mold temperature to 80 °C and packing time 25 s. These variations of injection conditions did not affect the fiber orientation distribution whatever the location or fiber concentrations. Therefore, in the following, the results for the standard condition only will be presented.

2.2. Measurement of fiber orientation

The most widely used technique for fiber orientation characterization in molded parts consists in observing a polished cross-section, either by optical or scanning electronic microscopy. These observations give a rough idea of the fiber state, and quantification is very important to compare efficiently the different patterns. Cylindrical fibers making a certain angle with respect to the cutting plane appear as ellipses. The measurement of the semi-axes of the ellipse allows the quasi-3D reconstruction of the fibers included within a cross-sectional area of material, whose size is typically cm×cm. Another technique is confocal laser scanning microscopy, which enables non-destructive 3D optical sectioning. The ellipses can be followed for a small distance, typically 20 μm, into the material. The displacement of the center of the ellipses leads to the fiber orientations. More recently, X-ray microtomography has been applied to reinforced thermoplastics. This technique enables the 3D reconstruction of most of the fibers within a small volume of material, whose size is of the order of 20 mm^3. From these X-ray data, complete fiber characterizations (including fiber orientation, length, curvature and fiber–fiber spatial statistics) can now be obtained. Reviews of all of these available techniques can be found in Ref. [2].

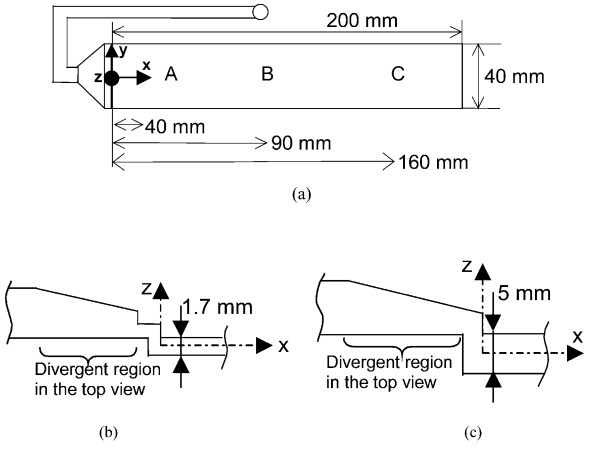

Fig. 1. Geometry and dimensions of the cavity, and positions of observation A, B and C (a). Gate region cross section in the plane (x, z) for a 1.7 mm plaque (b) and a 5 mm plaque (c).

Cross-sections in planes (y, z) perpendicular to the flow direction of the polyarylamide plaques were polished and observed by optical reflection microscopy. Fig. 2 shows a typical photomicrograph. It is possible to distinguish a thin central region, where the ellipses are elongated, and two large surface regions, where the fiber cross-sections are mostly circular. The measurement of the axes of the ellipses a and b leads to the orientation angles θ and ϕ (Fig. 3).

A concise representation of the orientation of a large population of fibers is the second order orientation tensor [3] defined as:

$$a_{ij} = \int_{\mathbf{p}} p_i p_j \psi(\mathbf{p}) \mathrm{d}\mathbf{p} \tag{1}$$

where $\mathbf{p}$ is a unit vector parallel to a fiber, with components p_i, which are related to the angles θ and ϕ, and $\psi(\mathbf{p})$ is the orientation distribution function, such that $\psi(\theta,\phi)\sin\theta \mathrm{d}\theta\mathrm{d}\phi$ is the probability of finding a fiber between angles θ and $\theta+\mathrm{d}\theta$ and ϕ and $\phi+\mathrm{d}\phi$.

The orientation tensor is symmetric and $a_{11}+a_{22}+a_{33}=1$. The diagonal components represent the strength of orientation in the respective directions. For instance, $a_{33}=0$ (respectively 1) means that fibers are perpendicular (respectively parallel) to direction 3. Random in space (respectively in plane) orientation leads to diagonal components equal to 1/3 (respectively 1/2).

There are several kinds of measurement and sampling errors which limit the precision of the image analysis system. The value of the angle ϕ is known with an uncertainty of π (Fig. 3). Consequently the sign of a_{13} and a_{23} is not known. Moreover, the probability of cutting a fiber is more likely when the fiber is perpendicular to the cutting plane than when it is parallel to it. Therefore, the contribution of a fiber of length L and diameter d with an angle θ with respect to the normal to the cutting plane must be weighted by a function $F(\theta)$ defined as [4]:

$$\frac{F(\theta)}{F(90)} = \frac{1}{\frac{L}{d}\cos\theta + \sin\theta} \tag{2}$$

where $F(90)$ is the weighting function at $\theta=90°$. The weight average value of a_{ij} obtained from the measurement of n

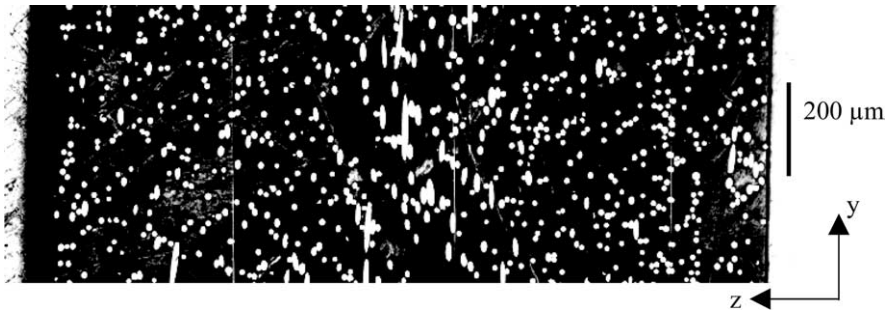

Fig. 2. Polished cross section in the (y, z) plane.

fibers of orientation p_i^k becomes:

$$a_{ij} = \frac{1}{n} \frac{\sum_{k=1}^{n} p_i^k p_j^k F(\theta_k)}{\sum_{k=1}^{n} F(\theta_k)} \quad (3)$$

The quantification was based on digitized images in the (y, z) plane of 20-mm wide cross sections across all of the thickness, corresponding to about 50,000 fibers for a thickness of 1.7 mm. The precise operations are described in Ref. [5].

2.3. Results

Values of a_{zz} are very close to 0 which means that fibers are almost parallel to the plane of the plaque. This is a classical result for most injected parts, where the thickness is small compared to the other dimensions. Moreover, non-diagonal components of the orientation tensor are close to zero, so that the (x, y, z) reference frame is a principal frame. Therefore, only a_{xx} will be represented in the following.

Fig. 4 shows the fiber orientation distribution for PAA50 for 1.1–5 mm thick plaques, in location C (Fig. 1 for the positions of observations). Above 3 mm a skin–core structure is observed. Similar results have been obtained for the other locations A and B. Both skin and core are quite well oriented, in the flow direction with a_{xx} larger than 0.8 for the skin, or perpendicular with a_{xx} around 0.2 for the core. For 1.1 and 1.7 mm thick plaque, the orientation distribution is very different. Fibers are quite well oriented in the flow direction throughout all the thickness.

The disappearance of the core region for thin plaques can be evaluated more precisely by the representation shown in Fig. 5. The grey level gives the local value of the component a_{xx} of the orientation tensor for about 50 fibers. Black is for fibers perpendicular to the x-direction, and white for fibers parallel. For 3 and 5 mm plaques, the core region appears continuous, even if variations between 0.1 and 0.5 can be observed. For the two other thicknesses, in the core, one observes dark regions with grey level corresponding to a_{xx} lower than 0.3, and large white regions corresponding to a_{xx} around 0.9. This variation does not appear on Fig. 4, because of averaging throughout the width of the sample (20 mm). Another strategy could have been to study several samples with a smaller width, and to average over these samples in order to have the same number of fibers and so the same sampling quality. The comparison of two samples shows that the positions of the clear and dark areas over the 20 mm width of the samples are not the same, so this methodology should have probably lead to the same kind of results.

The evolution of a_{xx} along the 1.7 mm thick plaque is presented in Fig. 6 for the three locations A, B, and C indicated in Fig. 1. For PAA50, fibers are oriented in the flow direction with a_{xx} included between 0.7 and 0.9 in the whole thickness, whatever the position along the plaque. For PAA30, large layers near the surface have an orientation parallel to the flow, with a_{xx} around 0.7–0.8, whereas in the

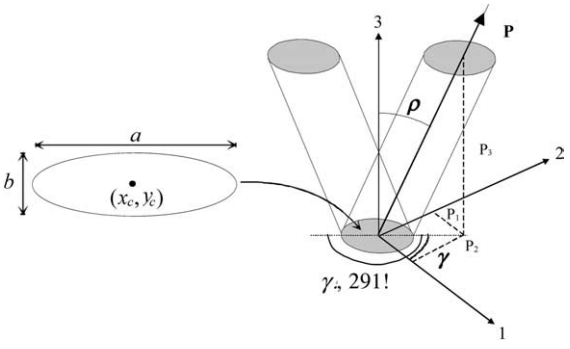

Fig. 3. Definition of the orientation angles (θ, ϕ) of a fiber.

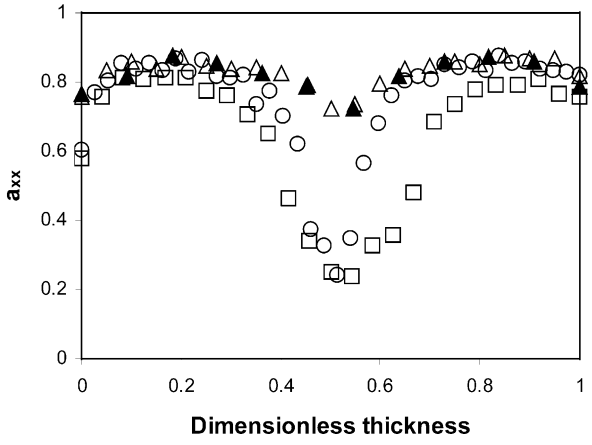

Fig. 4. Evolution of a_{xx} in the thickness for PAA 50 in position C for the four cavity thicknesses: 1,1 (▲), 1,7 (△), 3 (○) and 5 (□) mm.

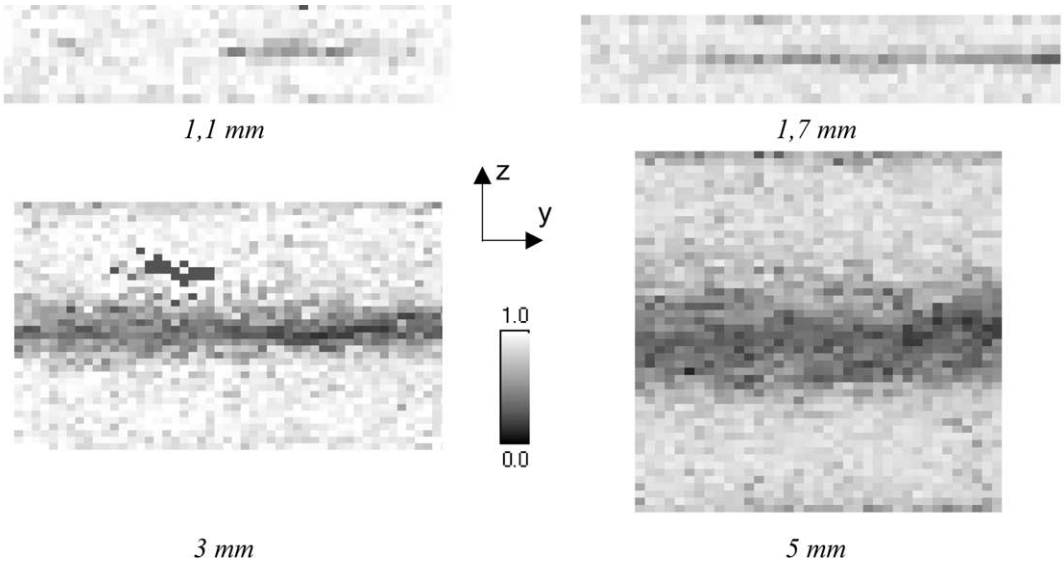

Fig. 5. Intensity of fiber orientation in the flow direction for four cavity thicknesses. White means $a_{xx}=1$, black $a_{xx}=0$. Position C, PAA 50. The width of the observed area in the y direction is around 10 mm.

center, the values are between 0.35 close to the gate and 0.5 far from it.

As shear flow in the plaque cannot explain the transverse orientation in the core for 3 and 5 mm PAA 50 plaques, and for all PAA 30 plaques, we have studied in more detail the entrance region. Fig. 7 shows a_{xx} values at the plaque entrance, that is for $x=5$ mm, for the PAA 50. A core region with orientation intermediate between planar isotropy ($a_{xx}=0.5$) and transverse to the flow direction is visible, especially for the thickest plaque. Observations show that this core orientation is created in the triangular region in the top view of the plaque (Fig. 1(a)), also called 'diverging region' on Fig. 1(b) and (c). Indeed, it is converging in the (x, z) plane, and diverging in the (x, y) plane. It is known that

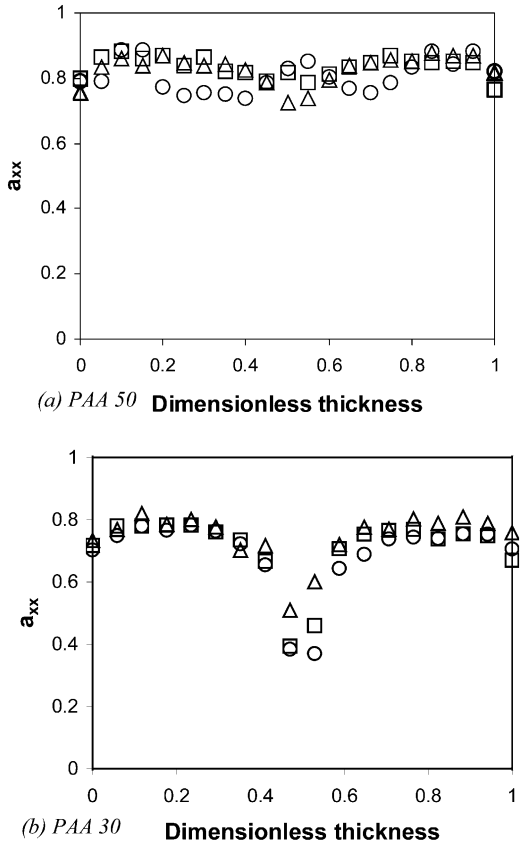

Fig. 6. Evolution of a_{xx} in the thickness for PAA 50 (a) and PAA 30 (b), for the 1.7 mm thick plaque, in positions A (○), B (□) and C (△).

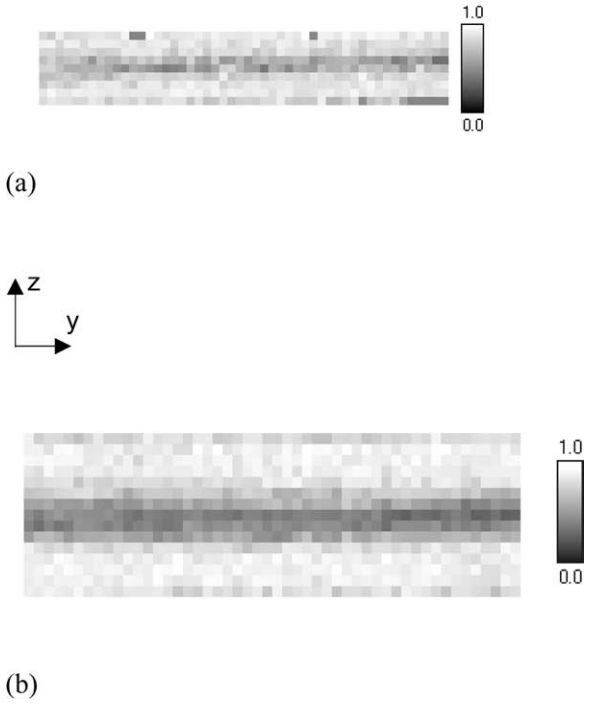

Fig. 7. Values of a_{xx} for the PAA 50, at $x=5$ mm from the plaque entrance, in the (y, z) plane. (a) 1.7 mm thick plaque. (b) 3 mm thick plaque.

a convergent (with positive elongational rate) leads to an orientation parallel to the flow, whereas a divergent (with negative elongational rate) leads to a perpendicular orientation. This last effect is predominant. The transverse orientation is not too much disturbed until the entrance of the plaque. Similar results have been observed for PAA 30.

After the gate, the flow is dominated by shear deformations. For the 3 and 5 mm thick plaques, they are not high enough to reorient fibers in the flow direction in the core, which explains why a_{xx} is around 0.2 in zone C for both materials (Fig. 8). For the thin plaques, the shear rate is much higher, and fibers get quickly reoriented in the flow direction, with a_{xx} larger than 0.7 in the core in location A and downstream (Fig. 6(a)). The behavior of the PAA 30 in the 1.7 mm plaque is very different. There is only a tendency of reorientation in the core, with a_{xx} between 0.35 and 0.5 (Fig. 6(b)).

Observations have also been made near position C, at $x=$ 160 and 5 mm from the plaque edges. For the PAA 50, and the 1.7 mm plaque, the intermittent core region visible on Fig. 5 disappears. All the fibers are aligned parallel to the wall, showing the effect of fiber–wall interactions.

3. Modeling of fiber orientation

Jeffery [6] obtained the equation of motion of a single particle in a Newtonian fluid. In a pure shear flow, fibers rotate periodically. The rotation velocity is high when fibers are perpendicular to the flow, and low when they are parallel. They spend much more time near the flow direction than perpendicular to it. In elongational flows, fibers tend to a stable equilibrium position. Folgar and Tucker [7] modified the previous theory by introducing a diffusion term accounting for fiber orientation in non-dilute concentration. The equation reads:

$$\frac{\mathrm{d}\mathbf{a}_2}{\mathrm{d}t} = \Omega\mathbf{a}_2 - \mathbf{a}_2\Omega + \lambda(\dot{\varepsilon}\mathbf{a}_2 + \mathbf{a}_2\dot{\varepsilon} - 2\dot{\varepsilon} : \mathbf{a}_4) + 2C_I\dot{\bar{\varepsilon}}(\mathbf{I} - 3\mathbf{a}_2) \tag{4}$$

where $\lambda = (r^2-1)/(r^2+1)$, and r is the fiber aspect ratio, $\boldsymbol{\Omega}$ and $\dot{\varepsilon}$ are the vorticity and rate of strain tensors, C_I is the interaction coefficient, $\mathbf{a}_4$ is the fourth order orientation tensor, which is defined as $a_{ijkl} = \int_{\mathbf{p}} p_i p_j p_k p_l \psi(\mathbf{p})\mathrm{d}\mathbf{p}$. In a shear flow, the orientation tends to a steady state. The orientation distribution is narrow for small C_I, and broad for high C_I.

There are two main issues concerning the orientation equation. First, $\mathbf{a}_4$ must be expressed as a function of $\mathbf{a}_2$ using a closure approximation. The quality of the results depends on this approximation. The simple quadratic closure approximation is exact when fibers are perfectly aligned, and the linear closure is exact for random orientation. More and more precise approximations have been developed, based on the natural [8] and orthotropic closures [9]. Second, C_I values must be specified for each material. It can be determined by fitting the computation to observations [7,10]. The values are in the range 10^{-2} to 10^{-4}. The relation between C_I and the suspension characteristics is not well established. C_I may depend on the inter-fiber spacing, and even on fiber orientation leading to anisotropic diffusivity [11–15].

The velocity gradients needed in Eq. (4) are usually obtained from classical flow computations based on an isotropic viscous behavior, namely a shear-thinning behavior. Most computations are based on the Hele Shaw equations for thin cavities (see for instance [8,16–18]). Full 3D computations are few in number [19].

Fig. 9 shows the comparison between the computation and the measurements shown in Section 2. The computation has been carried out with the MoldFlow software package, assuming the lubrication approximations in non-isothermal conditions. The value of C_I was obtained from the semi-empirical relation with the fiber concentration and

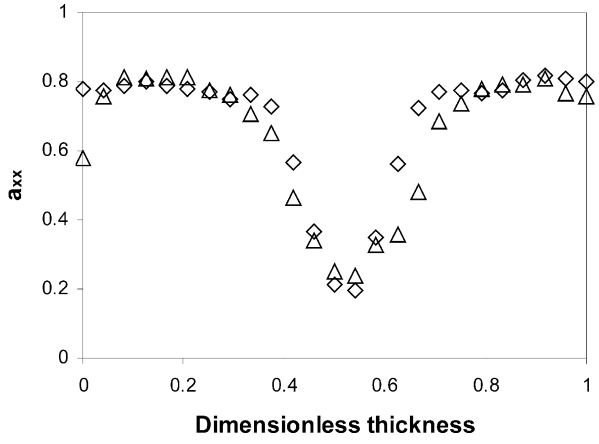

Fig. 8. Evolution of a_{xx} in the thickness in position C of the 5 mm plaque for PAA 50 (△) and PAA 30 (■).

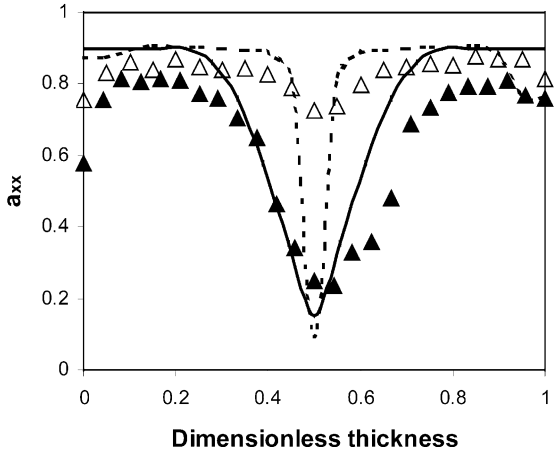

Fig. 9. Evolution of a_{xx} in the thickness in position C for PAA 50 for the 1.7 mm plaque, computed (- - -) and measured (△), and for the 5 mm plaque, computed (—) and measured (▲).

aspect ratio obtained by Bay [20]. A mean fiber aspect ratio of 20 has been used, so that C_I is 0.0018 for PAA30, and 0.0002 for PAA50. A hybrid closure approximation [21] has been used. The initial orientation is specified at the connection between the channel and the diverging region. It is referred as a 'standard' skin core orientation very similar to what have been experimentally obtained for the PAA 50 in position C for 5 mm plaques (Fig. 4). The sensitivity to this initial orientation is weak. For all the tested situations, the computation predicts that the fibers are almost in the plane of the plaque, with very low values of a_{zz}, in agreement with the observations. The variation of the molding parameters hardly changes the predicted orientation, as seen in the experimental data. For the 5 mm cavity, the computation predicts correctly the core region for both materials (Fig. 9 for the PAA50). The small difference in the level of a_{xx} in the surface can be reduced by modifying the interaction coefficient C_I, without any modification of the core region. For the 1.7 mm cavity, Fig. 9 shows that the computation is correct at the surfaces, but it predicts a core region which was not observed, except locally (Fig. 5). The disagreement may come from the thin flow approximation, which is unable to take into account the complex flow in the gate region between the feeding channel and the plaque, but also from the orientation equation itself. This is confirmed by the fact that in position A, that is close to the plaque entrance, for the 1.7 mm thickness sample PAA30, the computation predicts a very large core region, much larger than the observed one.

The fact that fiber orientation has no influence on the flow is an assumption. It has been shown that the rheology [22,23], and the velocity in an abrupt contraction [24], are affected by the orientation of the fibers. Most constitutive equations ([25,26] for reviews) taking into account the fibers assume a Newtonian behavior for the fluid, and dilute or semi-concentrated suspensions. However, molten thermoplastics exhibit shear thinning and are viscoelastic, and the fiber concentration is high (concentrated regime). They can be written as:

$$\sigma = -p\mathbf{I} + 2\eta_I[\dot{\varepsilon} + N_p\dot{\varepsilon} : \mathbf{a}_4 + N_s(\dot{\varepsilon}\mathbf{a}_2 + \mathbf{a}_2\dot{\varepsilon})] \quad (5)$$

η_I, N_p, N_s depend on the fluid viscosity, fiber aspect ratio, orientation and concentration (when the semi dilute regime is considered). η_I contains all the isotropic contributions from the fluid and the particles, and N_p and N_s contain anisotropic contributions from the particles. The parameters appearing in Eq. (5) can be obtained using rheological investigation [22], but they can be also theoretically estimated as a function of the fiber concentration and aspect ratio.

Fig. 10 shows the isovalues of the component of the orientation tensor corresponding to the flow direction (noted z) in the filling of a tube cavity. Considering long slender particles, $\lambda = 1$, N_s is taken equal to 0, and $N_p = 19.5$. This value is obtained with Dinh and Armstrong relation [27], for

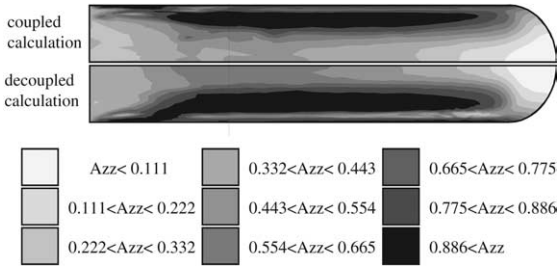

Fig. 10. Isovalues of fiber orientation tensor during filling of a tubular cavity.

aligned fibers of length 163 μm and diameter 7 μm, in a volume fraction 0.16. A Galerkin finite element method is used, and a penalty treatment of the incompressibility condition eliminates pressure as unknown [28]. The velocity is approximated using quadratic basis on six-nodes triangular elements. The flow domain evolution is obtained with an arbitrary Lagrangian Eulerian method. The temperature is also obtained by a Galerkin method. The orientation is determined by computing the generalized deformation tensor (see for instance [26] for the relation between orientation and this tensor) with a characteristic method coupled with the Galerkin method [29]. The diffusion term in Eq. (4) is not taken into account. The isotropic entrance orientation becomes a skin/core structure, except at the flow front, where the fountain flow takes place. The orientation at the front is rapidly frozen close to the cold mold, and this is the reason why in most observations there is a decrease of the orientation tensor component (Figs. 4, 6 and 8). Even in this simple case, there are some differences between the coupled and uncoupled flow and fiber orientation calculations. This is due to the fact that more the fibers are aligned with the flow direction, smaller their contribution to the stress field is. Fibers are oriented near the walls in the flow direction by the shear deformations, which are maximal here, and much less oriented in the core, where deformations are weak. There is, therefore, an equivalent viscosity gradient. The velocity profile is parabolic for a Newtonian behavior, and becomes flatter with an anisotropic behavior. Larger differences coming from the coupling can be expected in more complex 3D flows.

4. Conclusions

Even if basic flow induced fiber orientation phenomena are quite well understood, the details in actual injection molded components are not so easy to capture. Quantification of the observed orientation with the classical 2D method becomes more and more reliable, even if there are several sources of uncertainties. Fiber–fiber interactions in relation to the concentration, and fiber–wall interactions are key points which can change dramatically the orientation patterns. The importance of the gate has also been pointed out. Computer design tools are available, and they already

give valuable results. The limitations that have to be overcome originate not only in the standard fiber orientation equations but also in the kinematics computation. Nevertheless, these calculations can be coupled with an evaluation of the local elastic modulus in order to predict the mechanical properties of fiber reinforced composites.

Acknowledgements

The authors wish to thank MoldFlow, Schneider Electric and Bosch for technical and financial support, as well as the British–French integrated action program Alliance.

References

[1] Papathanasiou TD. Flow-induced alignment in injection molding of fiber-reinforced polymer composites. In: Papathanasiou TD, Guell DC, editors. Flow-induced alignment in composite materials. Cambridge: Woodhead Publishing Ltd; 1997. p. 113–65.
[2] Clarke A, Eberhardt C. Microscopy techniques for materials science. Cambridge: Woodhead Publishing Ltd; 2002.
[3] Advani AG, Tucker CL. J Rheol 1987;31(8):751–84.
[4] Bay RS, Tucker CL. Polym Eng Sci 1992;32(4):240–53.
[5] Eberhardt C, Clarke A, Vincent M, Giroud T, Flouret S. Compos Sci Technol 2001;61:1961–74.
[6] Jeffery GB. Proc R Soc London 1922;A102:161.
[7] Folgar F, Tucker CL. J Reinf Plast Compos 1984;3:98.
[8] Dupret F, Verleye V. Modelling the flow of fiber suspensions in narrow gaps. In: Siginer DA, De Kee D, Chhabra RP, editors. Advances in the flow and rheology of non-Newtonian fluids, Part B. Amsterdam: Elsevier; 1999. p. 1347–98.
[9] Cintra JS, Tucker CL. J Rheol 1995;39:1095–122.
[10] Bay RS. PhD Thesis, University of Illinois, Urbana-Champaign; 1991.
[11] Kamal MR, Mutel AT. Polym Compos 1989;10:337–43.
[12] Ranganathan S, Advani SG. J Rheol 1991;35:1499–522.
[13] Becraft ML, Metzner AB. J Rheol 1992;36:143.
[14] Stover CA, Koch DL, Cohen C. J Fluid Mech 1992;238:277–96.
[15] Phan-Thien N, Fan XJ, Tanner RI, Zheng R. J Non-Newtonian Fluid Mech 2002;103:251–60.
[16] Gupta M, Wang KK. Polym Compos 1993;14:367–82.
[17] VerWeyst BE, Tucker CL, Foss PH. Int Polym Proc 1997;12:238–48.
[18] Zheng R, Kennedy P, Phan-Thien N, Fan XJ. J Non-Newtonian Fluid Mech 1999;84:159–90.
[19] Kabanemi KK, Hétu J-F, Garcia-Rejon A. Int Polym Proc 1997;12: 182–91.
[20] Bay RS. PhD Thesis, University of Illinois, Urbana-Champaign; 1991.
[21] Advani SG, Tucker CL. J Rheol 1990;34:367–86.
[22] Ausias G, Agassant J-F, Vincent M, Lafleur PG, Lavoie PA, Carreau PJ. J Rheol 1992;36:525–42.
[23] Souloumiac B, Vincent M. Rheol Acta 1998;37:289–98.
[24] Lipscomb GG, Denn MM, Hur DU, Boger DV. J Non-Newtonian Fluid Mech 1988;26:297–325.
[25] Petrie CJS. J Non-Newtonian Fluid Mech 1999;87:369–402.
[26] Vincent M. Modelling of short fiber reinforced thermoplastics flows in polymer processing. In: Cunha AM, Fakirov S, editors. Structure development during polymer processing. Dordrecht: Kluwer; 2000. p. 345–63.
[27] Dinh SM, Armstrong RC. J Rheol 1984;28:207–27.
[28] Magnin B, Coupez T, Vincent M, Agassant JF. Numerical modeling of injection mold filling with an accurate description of the flow front. In: Chenot JL, Wood RD, Zienkiewicz OC, editors. Numerical methods in industrial forming processes. Rotterdam: Balkema; 1992. p. 365–70.
[29] Souloumiac B. PhD Thesis, Ecole des Mines de Paris, France; 1996.